FEM based Electromagnetic Signature Analysis of Winding Inter-turn Short-Circuit Fault in Inverter fed Induction Motor

Praveen Kumar N and Isha T B

***Abstract*—The intent of this paper is to analyze the electromagnetic signature of stator winding inter-turn short-circuit fault in a closed loop speed controlled Induction Motor (IM) employing Finite Element Method. Stator winding short-circuit nearly covers 21% of faults in IM. Diagnosing the inter-turn fault at an incipient stage is one of the challenging task in the area of fault detection of IM to prevent crucial damages in industrial applications. Also detecting the faults in inverter fed IM under variable speed applications under varying load is one of the major issues in industrial drives. As the signatures of electromagnetic field contains the entire data in association with the location of rotor, stator and mechanical parts of the motor, a regular monitoring of fields in the airgap can be used to diagnose the inter-turn fault in the stator winding of IM. In this direction, an IM is modeled with several inter-turn fault severities like 30 turns, 15 turns, 5 turns & 1 turn short using ANSYS Maxwell FEA tool and coupled with ANSYS Simplorer for loading arrangements. The PWM inverter with closed loop speed controlled strategy is implemented in Matlab Simulink and co-simulated with ANSYS Simplorer to integrate all the components in one common simulation platform environment for accurate design & analysis for realistic simulation. Several electromagnetic variables like flux density, flux lines and airgap flux density distribution over the machine are analyzed. The spatial FFT spectrum of radial component of flux density in the airgap contains the information related to the diagnosis of inter-turn fault at the incipient stage.**

***Index Terms*—Electromagnetic fields, finite element analysis, inter-turn fault, PWM inverter, radial flux density.**

I. INTRODUCTION

INDUCTION MACHINES (IM) are the most preferred in industry due to less maintenance, low cost and high reliability. IM are operated from pulse width modulated (PWM) inverters for adjustable speed applications. When the IM is supplied from PWM inverters, the stator windings are subjected to severe electrical stress due to semiconductor switching devices. Although mechanically robust, IM are vulnerable to several mechanical and electrical faults in the stator and rotor.

Manuscript was submitted for review on 12, June, 2018.

Praveen Kumar N, Department of Electrical and Electronics Engineering, Amrita School of Engineering, Coimbatore, Amrita Vishwa Vidyapeetham, India (n_praveenkumar@cb.amrita.edu).

Isha T B, Department of Electrical and Electronics Engineering, Amrita School of Engineering, Coimbatore, Amrita Vishwa Vidyapeetham, India (tb_isha@cb.amrita.edu).

Digital Object Identifier 10.30941/CESTEMS.2019.00041

According to a reliability study [1], around 21% of faults in IM occur in the stator winding. Faults in stator winding will start as an incipient minor inter-turn fault in a coil and in a very short time progresses into phase to phase or phase to ground faults. The root cause of inter-turn fault is due to thermal, environmental, mechanical and electrical stresses [2] working in the stator and these stresses get increased when the IM is supplied from PWM inverters [3].

Stator winding inter-turn fault originates with degradation of insulation generating hot spots leading to cataclysmic failure. Such conditions are periodically experienced by IM operated from PWM inverters because the nature of line voltage waveform generated will seriously stress the winding insulation. Detection of deterioration in stator winding at an early stage prevents the catastrophic damage and proper maintenance can be performed. The popular method used in industries for detecting faults in mains fed IM is motor current signature analysis (MCSA) [4], [5]. MCSA provide accurate results for mains fed IM, but for inverter fed, the FFT spectrum of line current will contain additional lower order harmonics due to high switching frequencies of the inverter causing an unreliable detection of faults. In industries due to wide spread usage of automation, speed of IM is controlled automatically by utilizing various closed loop speed control strategies for switching PWM inverters. The fault detection methods used for mains fed IM are not competent in closed loop speed controlled applications because the control techniques will tend to maintain normal operation of the drive even when fault occurs, masking the fault indicators [4].

Study of faults in IM can be performed through laboratory experiments or simulation based analysis. For economic and safety reasons, simulation based analysis is favored for the fault study of IM. Finite Element Method (FEM) based modeling is a preferred approach for electromagnetic field analysis of IM, specifically under fault conditions [3]. FEM is accurate, reliable and provides more definite information about the IM compared to analytical methods which consider only the linear effects of magnetic material properties. In [6], the author used FEM to diagnose stator winding fault of mains fed IM with 44 shorted turns by using discrete wavelet transform. An FEM analysis is carried out for induction generator with different shorted turns based on parameters like THD of faulty phase and Park's vector trajectory [7]. Inter-turn fault in mains fed IM with less than 5% of shorted turns is detected by employing

Park's transformation & cross wavelet transform on line current [8]. In [9], self and mutual inductances of mains fed IM is used to diagnose the inter-turn fault with 25% shorted turns in a phase using FEM. FEM is also used to detect the broken rotor bar faults in IM based on torque monitoring [10] and radial flux density of airgap [11]. Many research works available in the literature for diagnosis of stator winding inter-turn fault are mostly based on mains fed IM with more percentage of turns shorted in a phase. Very few works have been spotted for detection at the incipient stage of inter-turn fault & also for variable speed operation.

In this paper, an electromagnetic analysis is carried out for a closed loop speed controlled PWM inverter operated IM using FEM, which is modeled for inter-turn fault with several shorted turns in a phase ranging from 30 shorted turns to a single shorted turn at the incipient stage. Various parameters like speed, phase currents, flux line distribution, flux density distribution and radial airgap flux density in the airgap is analyzed. The IM model considered for the study is from ANSYS Maxwell FEA tool coupled with ANSYS Simplorer for loading arrangements. The PWM inverter with closed loop *V/f* control strategy is modeled in Matlab Simulink and co-simulated with ANSYS Simplorer. The work is also intented to integrate various environments like ANSYS Maxwell, Simplorer and Matlab Simulink in one collective platform for accurate design and analysis for realistic simulation.

II. Modeling Of Inter-Turn Fault In IM Using FEM And Calculation Of Radial Flux Density Using FEM

A 7.5 kW, 380 V, Y connected, 3φ, 4 pole IM model with 44 and 48 rotor & stator slots in ANSYS Maxwell as shown in Fig. 1 is considered for the study. There are 16 coils per phase and each coil in the model consists of 15 turns. The analysis is performed for various number of shorted turns involving 30 turns (12.5%), 15 turns (6.25%), 5 turns and 1 turn short-circuit. For implementing 30 turns, two complete coils and for 15 turns, one full coil is shorted. For implementing 5 turns and 1 turn short in a coil of Phase A, the particular coil branch is divided into one shorted winding and one non-shorted winding as indicated in Fig. 1. The coil branches will be connected in series for healthy condition and will be disconnected through a switch for short-circuit condition.

The radial component of flux density in the airgap of IM can be computed as,

$$B(\theta,t) = \Lambda(\theta,t)[F_1(\theta,t) + F_2(\theta,t)] \tag{1}$$

where Λ is the permeance of airgap per unit area, F_1 is the stator MMF, F_2 is the rotor MMF and θ is the geometrical angle. The permeance of airgap per unit area is the aggregate of average permeance, rotor and stator slot harmonic permeance and the reciprocal effect of rotor & stator [12],

$$\begin{aligned}\Lambda(\theta,t) = {} & \frac{\mu_o}{\delta_o K_c} + \sum_{k=1}^{\infty}\Lambda_{1,k}Cos(kN_s\theta) + \\ & \sum_{\ell=1}^{\infty}\Lambda_{2,\ell}Cos[\ell N_r(\theta-\omega_2 t)] + \\ & \sum_{k=1}^{\infty}\sum_{\ell=1}^{\infty}\Lambda_{1,2,k\pm\ell}Cos[(kN_s \pm \ell N_r)\theta - \ell N_r\omega_2 t]\end{aligned} \tag{2}$$

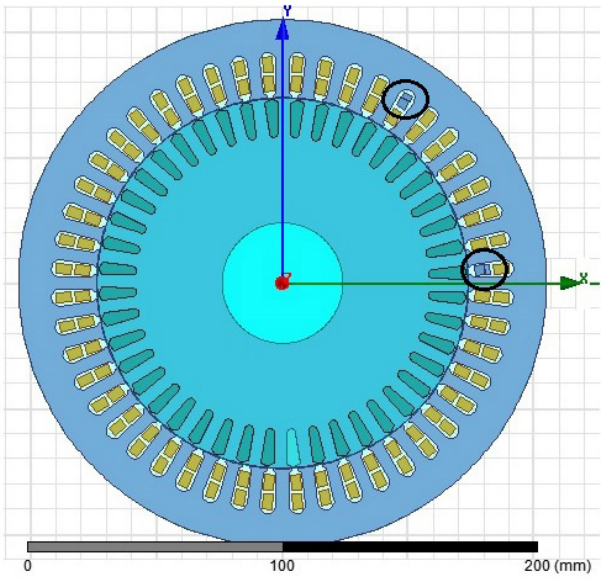

Fig. 1. IM model for inter-turn short-circuit fault.

where K_c is Carter's coefficient, δ_o is the length of the airgap, N_s and N_r is the number of stator and rotor slots, ω_2 is the rotor angular frequency, k and ℓ are integers associated with stator and rotor slots and Λ_1 & Λ_2 are partial permeances. The stator and rotor MMF of IM can be expressed as [13],

$$F_1(\theta,t) = \sum_{v=6k\pm1}^{\infty} F_{1mv}Cos(v\theta_e \pm \omega_1 t) \tag{3}$$

$$F_2(\theta,t) = \sum_{\mu=1}^{\infty} F_{2m\mu}Cos(\mu\theta_e \pm \omega_1 t - \varphi_\mu) \tag{4}$$

where F_{1mv} is the amplitude of stator fundamental MMF, v is the MMF spatial harmonic of stator, ω_1 is the angular frequency of stator, k is an integer, $F_{2m\mu}$ is the fundamental amplitude of rotor MMF, φ_μ is the reference angle between stator and rotor fundamental MMF, θ_e is the number of pole pair times geometrical angle and μ is the rotor MMF spatial harmonic given by,

$$\mu = \frac{kN_r}{P} \pm 1 \tag{5}$$

where P is the number of pole pairs. The IM simulated in FEM illustrates the electromagnetic analysis for non-conducting & conducting regions as [14],

$$-\nabla.(\frac{1}{\mu_o}\nabla A_z) = J_z \tag{6}$$

on airgap and stator slots, where A_z is the z component vector potential, and J_z is the current density of z component. For the stator and rotor iron parts,

$$-\nabla.(\frac{1}{\mu_i}\nabla A_z) = J_z \tag{7}$$

On the rotor conductors and shaft,

$$-\nabla.(\frac{1}{\mu_o}\nabla A_z) + \sigma\frac{\partial A_z}{\partial t} = \frac{\sigma\Delta V}{l_m} \tag{8}$$

where σ is the conductivity of rotor conductors and shaft, ΔV is the differential voltage of the regions conducting and the motor length is l_m. The magnetic flux density distribution is expressed as,

$$(B_x, B_y) = (\frac{\partial A_z}{\partial y}, -\frac{\partial A_z}{\partial x}) \quad (9)$$

The radial component of airgap flux density B_r represented in cylindrical co-ordinate as a function of scalar & vector field as [15]

$$B_r = \overline{B}.\overline{i_r} = (B_x \overline{i_x} + B_y \overline{i_y}).(\cos[\phi]\overline{i_x} + \sin[\phi]\overline{i_y}) \quad (10)$$

$$\overline{B_r} = B_r \overline{i_r} = B_r(\cos[\phi]\overline{i_x} + \sin[\phi]\overline{i_y}) \quad (11)$$

in which ϕ is the anti-clockwise angle of a stator tooth center corresponding to the positive horizontal axis.

III. Electromagnetic Field Analysis Of IM For Various Turns Shorted In The Stator Winding

Fig. 2 shows the implementation of inter-turn short-circuit fault in the stator winding by integration of co-simulation between ANSYS Maxwell, Simplorer and Matlab Simulink. The FEM model of IM in ANSYS Maxwell is co-simulated with Simplorer for loading and supply arrangements. The PWM inverter with closed loop *V/f* speed control technique is implemented in Matlab Simulink and co-simulated with ANSYS Simplorer. The data is exchanged between Simplorer and Simulink through a special function called Ansoft S Function in Simulink. The pole voltages (V_a, V_b, V_c) of voltage source inverter modeled in Simulink is imported to the IM terminals (Phase A, Phase B, Phase C) in Simplorer and the measured shaft speed from Simplorer is fed to Simulink. The IM is started on no load with a reference speed of 1440 rpm and after a certain time a change in speed of 1300 rpm is applied. Then the machine is applied with a load torque of rated value 40 Nm and after a certain interval the fault is implemented on the stator winding through switching action and the machine is made to run with less number of turns in Phase A.

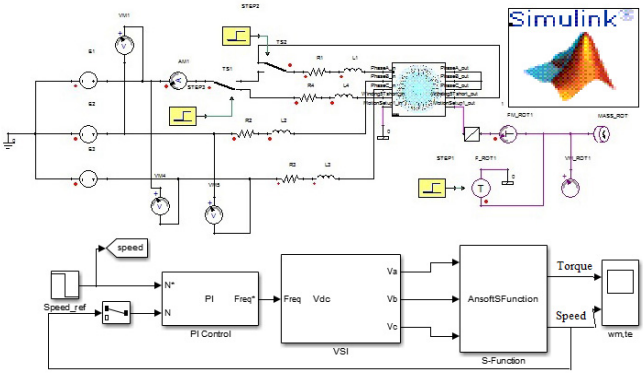

Fig. 2. Co-simulation between ANSYS Maxwell, Simplorer and Matlab Simulink for implementing closed loop *V/f* speed control for inter-turn fault.

Fig. 3 depicts the speed of the IM for 30 turns, 15 turns, 5 turns & 1 turn inter-turn short in Phase A winding. For 30 turns and 15 turns short, the IM is started healthy on no load with a speed of 1440 rpm & the speed is reduced to 1300 rpm at t=0.5s, the machine is applied with rated value of torque at t=0.8s and the short-circuit is implemented at t=1.8s. It can be seen from Fig. 3(a) and Fig. 3(b), at the instant of short-circuit, slight oscillations are noticed in the speed, magnitude of which depends upon the severity of the fault. Even though the speed control loop is acting, the percentage (12.5% & 6.25%) turns shorted are high enough to cause the oscillations. For 5 turn and 1 turn short, the IM is started on no-load and the speed is reduced to 1300 rpm at t=0.8s, and rated load is applied at t=1.4s, finally inter-turn short is implemented at t=2.6s. Since the number of turns shorted is very fewer, the speed control loop is able to keep the oscillations under control as seen from Fig. 3(c) and Fig. 3(d).

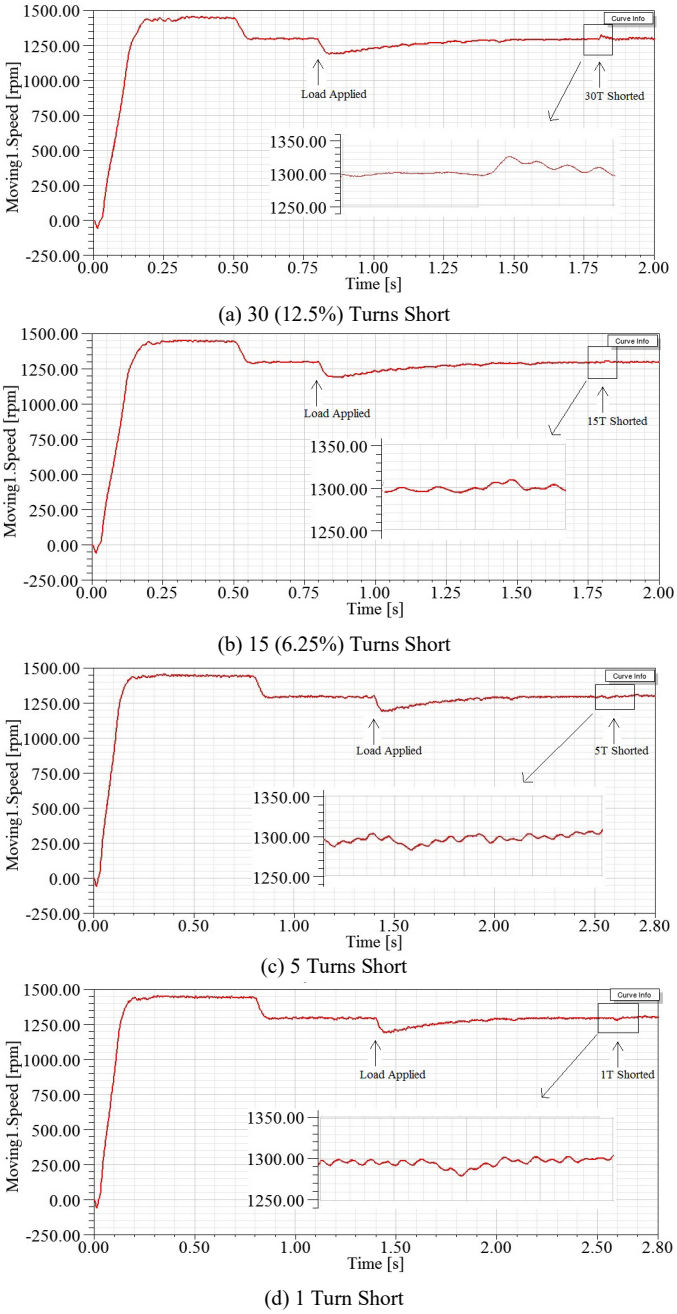

(a) 30 (12.5%) Turns Short

(b) 15 (6.25%) Turns Short

(c) 5 Turns Short

(d) 1 Turn Short

Fig. 3. Speed of IM for various inter-turn fault severities.

Fig. 4 illustrates the Phase A current where short-circuit is implemented in the coils of IM. Under healthy condition the machine takes a rated rms current of 14.26A and a peak value

of around 20.16A. For 30 turns and 15 turns short, the current increases rapidly at the instant of short-circuit which can be seen from Fig. 4(a) and Fig. 4(b). The peak current ripple increases nearly around 50% for 30 shorted turns and around 20% for 15 shorted turns. The increase in current ripples will be reflected as sudden transient torque oscillations which may possibly cause damages to the motor. In case of 5 turn and single turn short-circuit, the increase in current is negligible which can be seen from Fig. 4(c) and Fig. 4(d). It is very difficult to detect the incipient inter-turn fault for a closed loop speed controlled IM drive based on motor currents because the magnitude of the fault currents will be of appreciable value only when the number of shorted turns is around above 5%.

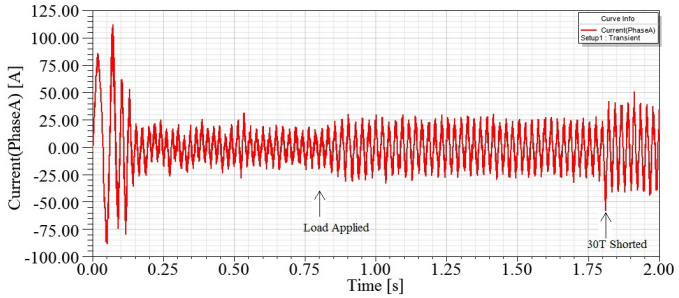

(a) 30 (12.5%) Turns Short

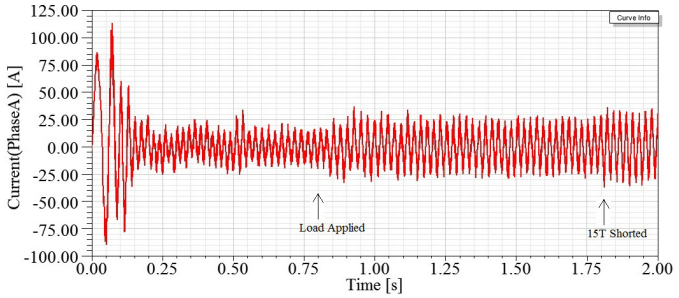

(b) 15 (6.25%) Turns Short

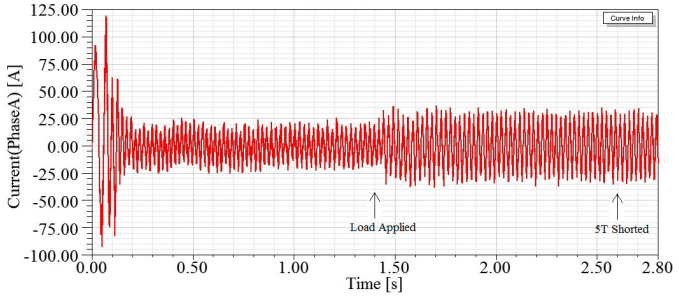

(c) 5 Turns Short

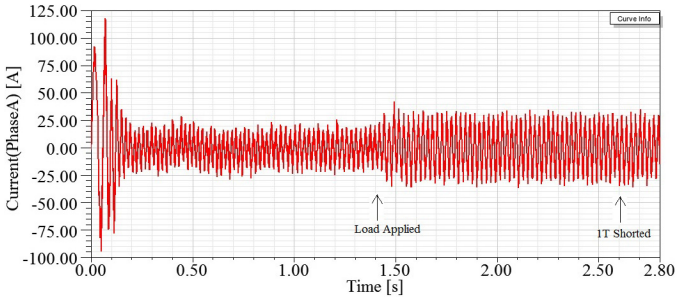

(d) 1 Turn Short

Fig. 4. Phase A Current of IM for various inter-turn fault severities.

Fig. 5 portrays the distribution of flux lines in IM under healthy and faulty condition. The distribution of flux lines around the IM under healthy condition at rated load is symmetric over the pole pitch as in Fig. 5(a). The poles are geometrically positioned at a magnetic axis of $360^{\circ}/2P$, where P is the number of pole pairs of the machine. When an inter-turn short occurs, the magnetic poles gets deformed due to the asymmetry in the magnetic field caused by the fault just after the instant of short-circuit as seen in Fig. 5(b) and Fig. 5(c) for 30 turns & 5 turns short under rated load. More dissymmetry in the distribution of magnetic flux lines is noticed for 30 shorted turns compared to 5 turns short. For single turn short, the distribution just after the instant of short-circuit is shown in Fig. 5(d). A very slight dissymmetry at the shaft center is noticed for incipient fault condition. So the distortion in the flux line distribution over the machine starts momentarily at the incipient stage of the fault and it widely deepens based on the fault severity. The distribution of magnetic flux density for healthy and faulty IM is depicted in Fig. 6. Compared to the symmetric distribution of healthy motor, a slight irregularity towards saturation is noticed near the shorted coil which is indicated for single turn short IM.

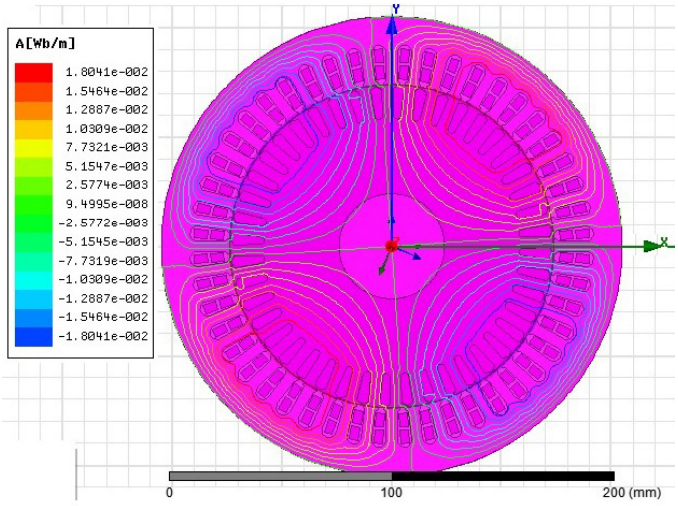

(a) Healthy Motor

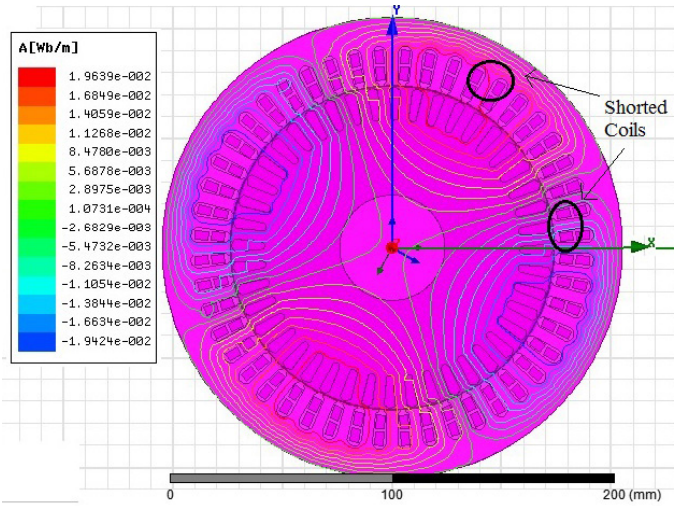

(b) 30 Turns Short

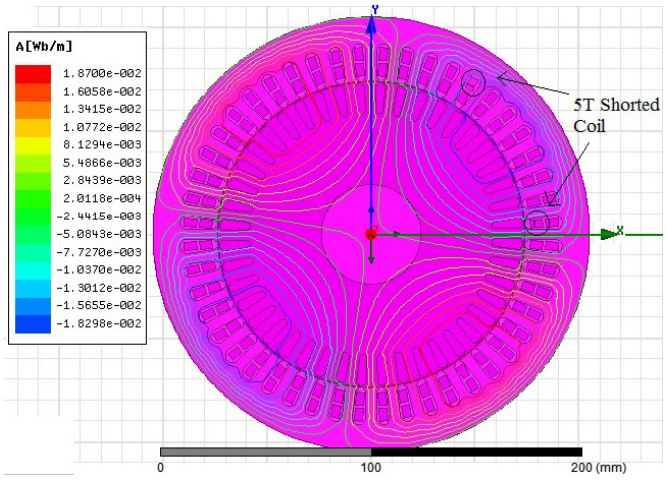

(c) 5 Turns Short

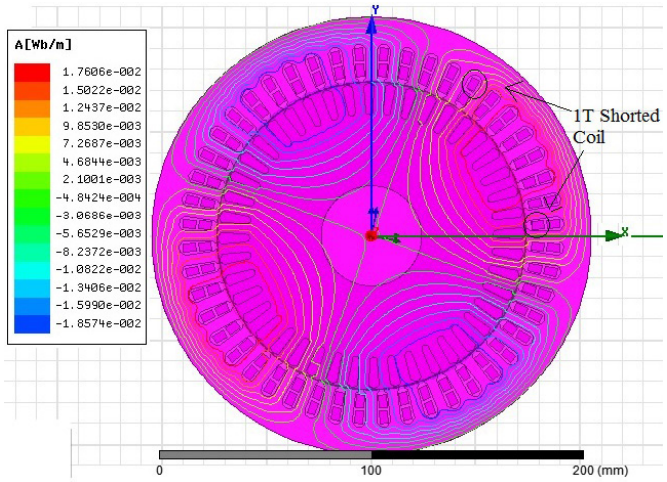

(d) 1 Turn Short

Fig. 5. Flux line distribution of IM for various inter-turn fault condition.

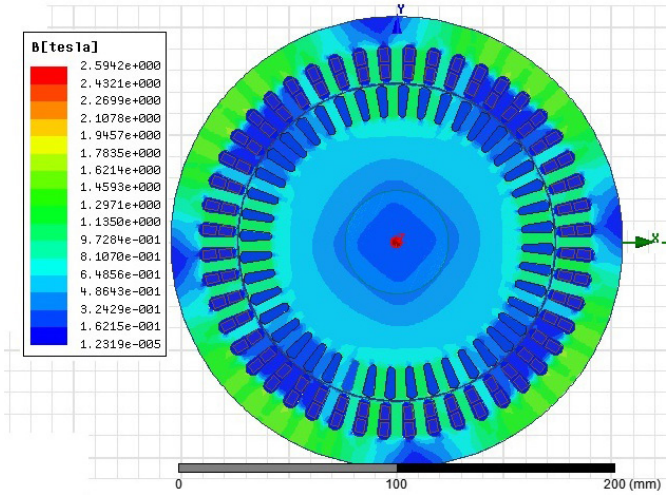

(a) Healthy Motor

IV. Radial Airgap Flux Density Analysis

The radial flux density in the airgap with respect to its radial distance for healthy and faulty IM is calculated from (10) and (11) and its spatial FFT spectrum is plotted. Fig. 7 exhibits the airgap radial flux density & its spatial FFT spectrum for a

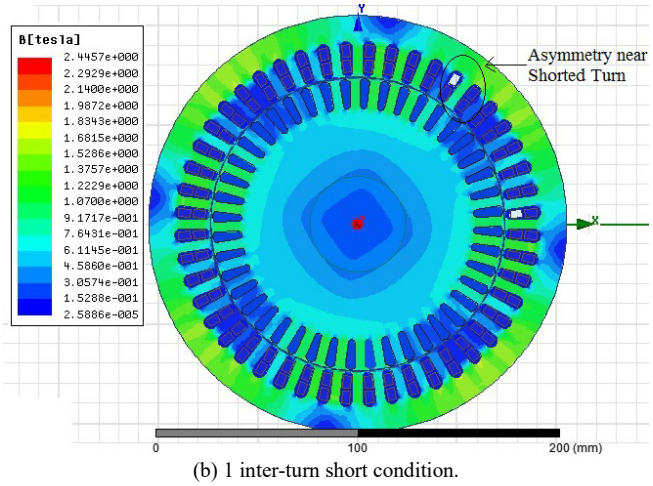

(b) 1 inter-turn short condition.

Fig. 6. Flux density distribution over the IM.

healthy IM under rated load condition. It bears the resemblance of a sinusoid with two electrical cycles for a 4 pole machine. The radial component of airgap field comprises of fundamental component, stator and rotor MMF harmonic components and also the permeances of rotor and stator slots. The amplitude of fundamental component for a healthy motor is around 0.57 Wb/m^2 under rated load condition. In the spatial FFT spectrum, apart from the fundamental the harmonics around a radial distance of 100 mm and 200 mm have appreciable magnitude.

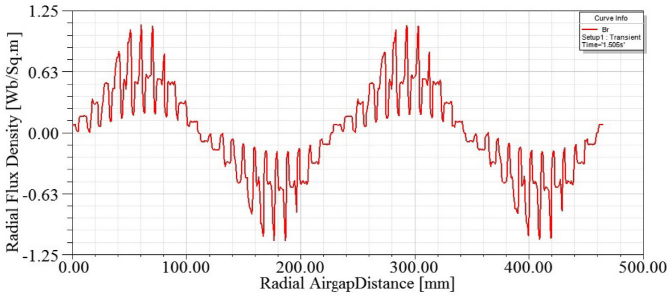

(a)

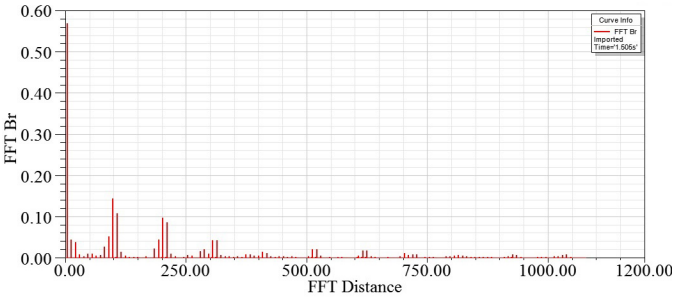

(b)

Fig. 7. (a) Airgap Radial Flux Density of Healthy Motor (b) Spatial FFT Spectrum of Healthy Motor

The airgap radial flux density and its spatial FFT spectrum for 30 turns and 15 turns short at the instant of short-circuit is presented in Fig. 8 and Fig. 9. The dissymmetry in the flux density caused by the inter-turn fault is indicated and it gets reflected as noise with additional harmonics in the spatial FFT spectrum compared to healthy motor. Fig. 10 and Fig. 11 shows the airgap flux density and its FFT spectrum for 5 turns and 1 turn short at the instant of fault. Since the number of turns shorted is very less and the fault is at the incipient stage, a slight

non-uniformity is noticed in the radial flux density and the harmonic noise content in the spatial FFT spectrum is very minimal.

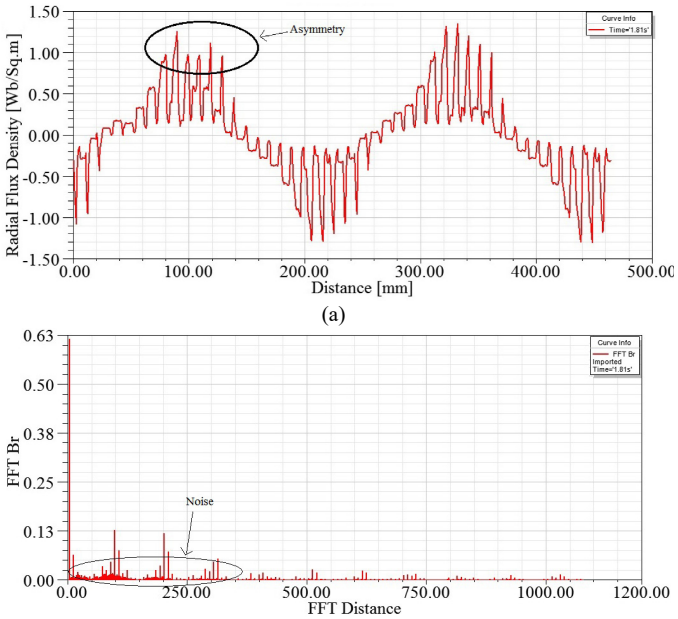

Fig. 8. (a) Airgap Radial Flux Density of 30 (12.5%) Turns Shorted Motor (b) Spatial FFT Spectrum of 30 Turns Shorted Motor

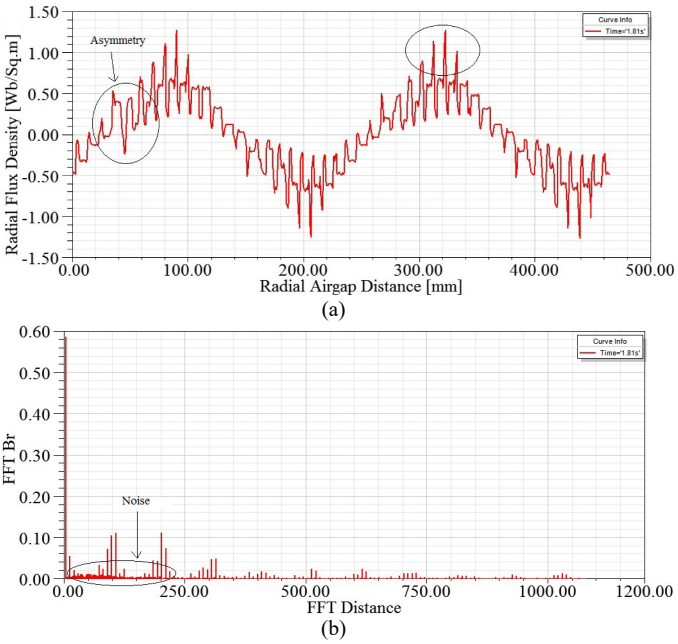

Fig. 9. (a) Airgap Radial Flux Density of 15 (6.25%) Turns Shorted Motor (b) Spatial FFT Spectrum of 15 Turns Short Motor

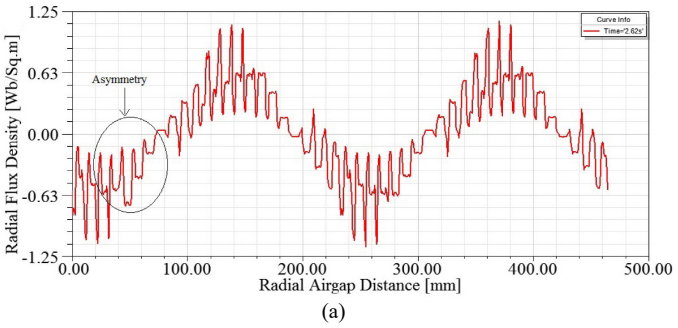

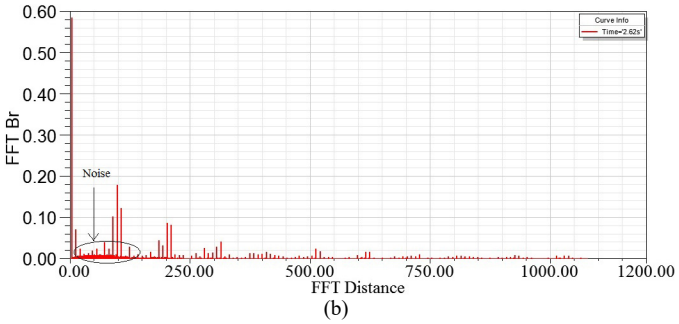

Fig. 10. (a) Airgap Radial Flux Density of 5 Turns Shorted Motor (b) Spatial FFT Spectrum of 5 Turns Shorted Motor

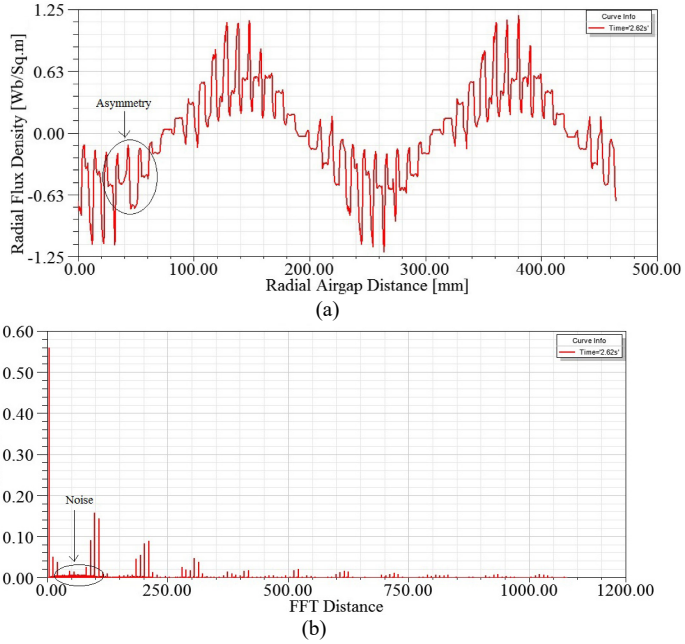

Fig. 11. (a) Airgap Radial Flux Density of 1 Turn Shorted Motor (b) Spatial FFT Spectrum of 1 Turn Shorted Motor

Let n be the number of harmonics present in the spatial FFT spectrum of healthy motor above an appreciable magnitude of 0.002 Wb/m^2. The amount of noise added to the spatial FFT spectrum increases by an amount of 75.5% for single inter-turn short fault. The noise further increases to 78.5% for 5 turn fault and to 90% for 15 turns short and finally to 103% for 30 turns short as seen in Table I. Thus the noise content in the spectrum escalates with the severity of the inter-turn fault. It is very difficult to detect changes in parameters like speed, currents or torque in case of the fault at the incipient stage, only changes noticed after the fault escalates to a certain level. But in case of inter-turn fault at the incipient stage, even though a single turn is shorted, gets reflected in the radial flux density of the airgap as additional harmonic noise content which can be seen from the spatial FFT spectrum.

TABLE I
NOISE PERCENTAGE IN RADIAL AIRGAP FLUX DENSITY FFT SPECTRUM FOR DIFFERENT INTER-TURN SHORT COMPARED TO HEALTHY INDUCTION MOTOR

Sl. No	***Motor Condition***	***Noise added to FFT Spectrum in Percentage***
1.	Healthy	Nil
2.	1 Turn Short	75.5

SI. No	*Motor Condition*	*Noise added to FFT Spectrum in Percentage*
3.	5 Turns Short	78.5
4.	15 Turns Short	90
5.	30 Turns Short	103

V. CONCLUSION

In this paper, an electromagnetic analysis is performed using FEM to study various parameters of closed loop speed controlled IM under different inter-turn short-circuit fault conditions. An IM is modeled for several inter-turn faults in ANSYS Maxwell coupled with ANSYS Simplorer for supply and load arrangements and co-simulated with Matlab Simulink for implementing closed loop speed controlled strategy. It is hard to notice changes in parameters like speed, current or torque at the incipient stage of inter-turn fault until the fault develops to a certain level. But a slight asymmetry is noticed in the flux lines and flux density distribution around the machine at the incipient stage compared to healthy motor. Also a slight non-uniformity is noticed in the radial flux density distribution of the airgap even for a single inter-turn fault compared to a healthy one and it gets reflected as additional harmonic noise content in the spatial FFT spectrum of airgap flux density. Compared to the healthy motor, 75.5% of noise is added to spatial FFT spectrum for single inter-turn short which finally increases to 103% for 30 turns short motor. The harmonic noise content escalates with the increase in number of shorted turns of inter-turn fault.

REFERENCES

[1] Bonnett, A.H.; Yung, C., "Increased Efficiency Versus Increased Reliability," *in Industry Applications Magazine, IEEE,* vol. 14, no. 1, pp. 29-36, Jan.-Feb. 2008.

[2] Bonnett, A.H.; Soukup, G.C., "Cause and analysis of stator and rotor failures in three-phase squirrel-cage induction motors," *in Industry Applications, IEEE Transactions on* , vol. 28, no. 4, pp. 921-937, Jul/Aug. 1992.

[3] B. Vaseghi, N. Takorabet, and F. Meibody-Tabar, "Transient Finite Element Analysis of Induction Machines with Stator Winding Turn Fault," *Progress In Electromagnetics Research*, Vol. 95, 1-18, 2009.

[4] Bellini, A.; Filippetti, F.; Tassoni, C.; Capolino, G.-A., "Advances in Diagnostic Techniques for Induction Machines," *in Industrial Electronics, IEEE Transactions on* , vol. 55, no. 12, pp. 4109-4126, Dec. 2008.

[5] M. Riera-Guasp, J. A. Antonino-Daviu and G. A. Capolino, "Advances in Electrical Machine, Power Electronic, and Drive Condition Monitoring and Fault Detection: State of the Art," in *IEEE Transactions on Industrial Electronics*, vol. 62, no. 3, pp. 1746-1759, Mar. 2015.

[6] Mohammed, O.A., Abed, N.Y., and Ganu, S., "Modeling and Characterization of Induction Motor Internal Faults Using Finite-Element and Discrete Wavelet Transforms," *in Magnetics, IEEE Transactions on* , vol. 42, no. 10, pp. 3434-3436, Oct. 2006.

[7] Y. Chen, L. Wang, Z. Wang, A. U. Rehman, Y. Cheng, Y. Zhao, and T. Tanaka, "FEM simulation and analysis on stator winding inter-turn fault in DFIG," in *2015 IEEE 11th International Conference on the Properties and Applications of Dielectric Materials (ICPADM)*, Sydney, NSW, July 2015, pp. 244-247.

[8] Das, S., Purkait, P., Dey, D., Chakravorti, S., "Monitoring of inter-turn insulation failure in induction motor using advanced signal and data processing tools," *in Dielectrics and Electrical Insulation, IEEE Transactions on* , vol. 18, no. 5, pp. 1599-1608, October 2011.

[9] Babak Vaseghi, Noureddine Takorabet and Farid Meibody-Tabar, "Stator turn fault study and parameter extraction of induction machines using FEM," *COMPEL - The international journal for computation and mathematics in electrical and electronic engineering*, vol. 29, no. 3, pp. 885-899, 2010.

[10] Gyftakis, K.N.; Spyropoulos, D.V.; Kappatou, J.C.; Mitronikas, E.D., "A Novel Approach for Broken Bar Fault Diagnosis in Induction Motors Through Torque Monitoring," in *Energy Conversion, IEEE Transactions on* , vol. 28, no. 2, pp. 267-277, Jun. 2013.

[11] Praveen Kumar N and Isha T B, "Electromagnetic field analysis of 3-Phase induction motor drive under broken rotor bar fault condition using FEM," *2016 IEEE International Conference on Power Electronics, Drives and Energy Systems (PEDES)*, Trivandrum, 2016, pp. 1-6.

[12] Sandarangani, C, *Electrical Machines–Design and analysis of induction and permanent magnet motors,* Royal Institute of Technology, Stockholm." (2000): 08-07.

[13] Boldea I, Nasar SA, *The induction machine handbook*, CRC press; 2010 Dec 12.

[14] Martinez, Jose Luis, Anouar Belahcen, and Antero Arkkio, "Combined FE and two dimensional spectral analysis of broken cage faults in induction motors." *Industrial Electronics Society, IECON 2013-39th Annual Conference of the IEEE*, Vienna, Austria, 2013, pp. 2674-2679.

[15] Praveen Kumar N, Isha T B and Balakrishnan P, "Radial electro-magnetic field analysis of induction motor under faulty condition using FEM," *2016 Biennial International Conference on Power and Energy Systems: Towards Sustainable Energy (PESTSE)*, Bangalore, 2016, pp. 1-6.

Praveen Kumar N received the B.E. degree in electrical & electronics engineering in 2004 and the M.Tech degree in power electronics from Amrita Vishwa Vidyapeetham, Coimbatore, India, in 2007. He is currently pursuing the Ph.D. degree in electrical engineering at Amrita Vishwa Vidyapeetham, Coimbatore, India.

He has an industrial experience of nearly four years in the field of electric motor drives. His research interest includes fault diagnosis in induction motor drives, electromagnetic field analysis of induction motor drives during several fault conditions, finite element analysis and power electronics.

Isha T B received her B. Sc degree in electrical engineering from Kerala University, India in 1982, M.Tech degree in power electronics from Regional Engineering College, Calicut, India in 1990 and Ph.D. degree from Indian Institute of Technology, Kharagpur, West Bengal, India in 2000.

She has been into teaching profession since 1983. She had served in several Engineering colleges. Since 2004, she is working as a professor in the Department of Electrical and Electronics Engineering at Amrita Vishwa Vidyapeetham, Coimbatore, India. Her research interest includes power electronics and drives, special machines, energy conversion systems and control systems. She had authored and co-authored several papers in National and International Journals and Conferences and completed several sponsored projects.